Development of a High-Propellant Throughput Small Spacecraft Electric Propulsion System to Enable Lower Cost NASA Science Missions

Gabriel F. Benavides[1], Hani Kamhawi[2], Thomas M. Liu[3], Luis R. Pinero[4], Timothy R. Verhey[5], Corey R. Rhodes[6], John T. Yim[7], Jonathan A. Mackey[8], Timothy G. Gray[9], and Naia I. Butler-Craig[10]
NASA Glenn Research Center, Cleveland, OH, 44135, USA

James L. Myers[11] and Arthur G. Birchenough[12]
Vantage Partners, LLC, Brook Park, OH, 44142, USA

This paper describes recent progress at the NASA Glenn Research Center (GRC) in the development and demonstration of an integrated high-propellant throughput small spacecraft electric propulsion (HT-SSEP) system based on a Hall-effect thruster. A center-mounted cathode and an innovative magnetic circuit topology were implemented in the design of the Hall-effect thruster to achieve high-propellant throughput, high performance, and efficient packaging. To minimize technical risk, the HT-SSEP development approach sought to limit design features and materials to those with a clear path-to-flight. A propellant throughput capability of greater than 100 kg at a minimum thruster efficiency of 50% was targeted. The proof-of-concept NASA-H64M laboratory model (LM) thruster was designed, fabricated, and tested at GRC in fiscal year 2018. The thruster development leveraged heritage Hall-effect thruster design and manufacturing processes wherever appropriate. Recent NASA advances in Hall-effect thruster technology were also leveraged. A scalable discharge power supply (DPS) capable of powering the H64M-LM was developed, then demonstrated as part of an integrated system test. The DPS uses commercial off-the-shelf components with spaceflight equivalents. A keeper supply with DC ignitor was breadboarded, then demonstrated with a laboratory cathode. Finally, feed system trade studies were performed to ascertain what feed system architecture might be appropriate for an HT-SSEP system. This paper details the motivations for the project, the development approach, the chosen sub-system architectures, design considerations, and test results.

I. Introduction

NASA is well-positioned to expand the utilization of lower-cost small spacecraft beyond low earth orbit (LEO) by developing a high-performance and high-propellant throughput small spacecraft electric propulsion (HT-SSEP) system leveraging NASA advances in Hall-effect thruster technology. By doing so, NASA can advance its strategic goal to increase the use of small spacecraft to accomplish its science goals [1]. The lower development and launch

[1] Research AST, Electric Propulsion Systems Branch, AIAA Senior Member.
[2] Research AST, Electric Propulsion Systems Branch, AIAA Associate Fellow.
[3] Research AST, Electric Propulsion Systems Branch, AIAA Member.
[4] Research AST, Electric Propulsion Systems Branch.
[5] Research AST, Electric Propulsion Systems Branch.
[6] Research AST, Electric Propulsion Systems Branch.
[7] Research AST, Electric Propulsion Systems Branch.
[8] Research AST, Electric Propulsion Systems Branch AIAA Member.
[9] Research AST, Electric Propulsion Systems Branch.
[10] Student Trainee, Science & Space Technology Systems Branch.
[11] Mechanical Engineer V, Thermal Systems & Transport Processes Branch.
[12] Systems Engineer V, Power Management & Distribution Branch.

costs of smaller spacecraft (< 500 kg) have the potential to increase the cadence of NASA missions and facilitate novel missions requiring numerous spacecraft flying in formations, swarms, or constellations. Before achieving this reality, technical deficiencies with state-of-the-art (SOA) on-board SSEP must be overcome, including technology readiness level (TRL), specific impulse, and/or total propellant throughput capability [2].

Specific impulse I_{sp} is a measure of the thrust T generated by a propulsion system for a given mass flow of propellant.

$$\boldsymbol{I_{sp} = {}^{T}/_{\dot{m} g_0}} \tag{1}$$

Total propellant throughput is the total mass of propellant a thruster can process over its lifetime. The combination of specific impulse and total propellant throughput defines the maximum total impulse I_T an on-board propulsion system can impart on a spacecraft over its lifetime.

$$\boldsymbol{I_T = \int_0^{t_f} T dt = \int_0^{t_f} I_{sp} \dot{m} g_0 dt} \tag{2}$$

For a spacecraft of fixed mass, the greater the total impulse capability of the propulsion system, the greater the spacecraft's capability becomes to independently carry out challenging propulsive tasks, such as orbit raising, inclination changes, achieving planetary escape velocities, and orbit capture.

Historically, these onboard propulsion systems have relied on energy releasing chemical reactions to power the propulsive engines. The most efficient chemical engines exhaust propellant at over 4 km/s to generate thrust. On the other hand, propellant accelerated by solar electric propulsion (SEP) can achieve velocities in excess of 40 km/s. In SEP, solar panels convert energy radiated from the sun into electrical energy. The propulsion system then converts the electrical energy into thrust by electrothermal, electromagnetic, or electrostatic processes [3]. The ability to achieve propellant velocities an order of magnitude greater than chemical systems permit SEP spacecraft to perform similar missions with as little as 10% the propellant mass [4]. Such a massive reduction in propellant mass, compared to a chemical system with comparable propulsive capability, can greatly reduce both the size and launch cost of spacecraft. For these benefits, a growing percentage of large commercial spacecraft are now employing SEP in near-Earth orbits. Similarly, NASA seeks to benefit from advanced SSEP technologies to perform its science goals at lower cost. If SEP can be effectively miniaturized for small spacecraft without significant loss of performance or lifetime, it could usher a paradigm shift through increasing access to space beyond Earth orbits.

Toward this end, in fiscal year 2018, the NASA Space Technology Mission Directorate (STMD) funded the Sub-Kilowatt Electric Propulsion (SKEP) project through its Game Changing Development (GCD) program. The SKEP project aimed to develop an electric propulsion system (i.e., thruster design, power processing unit design, and feed system concept) at a power, mass, volume, and cost commensurate with small spacecraft limited resources, but preserving substantial performance, propellant throughput, and reliability of the state-of-the-art higher power SEP systems. The project leveraged many recent advancements in solar electric propulsion technologies, often resulting from previous NASA investments, and achieved a successful low-power, high-performance HT-SSEP integrated system demonstration (i.e., thruster operated with discharge power supply). The HT-SSEP system was designed, manufactured, and demonstrated at the NASA Glenn Research Center (GRC) in Cleveland, Ohio. GRC is the lead NASA center for solar electric propulsion. GRC performs in-house SEP technology development activities and oversees SEP contracted efforts.

II. Stakeholders

The project was motivated by the observation that NASA small spacecraft have the potential to perform a wide range of scientifically compelling missions beyond Earth orbits, at lower cost than historically achievable, should a flight-qualified HT-SSEP system become available. GRC recognized that recent NASA investments in high-power Hall-effect thruster technology may now make such miniaturization possible without significant loss of performance as common amongst the SOA low-power systems. In short, the SKEP project began as a technology push.

As a consequence of a technology push, rather than mission pull, the stakeholders are not well defined in advance of receiving project approval to proceed (ATP). In order to ensure the SKEP team was developing the right technology (i.e. size, power, thrust, interfaces, etc.), an early project task was to identify credible stakeholders willing to provide immediate feedback on the HT-SSEP concept and requirements. The project sought stakeholders internal to NASA as well as feasible end-users from domestic industry. The Planetary Sciences Division (PSD) within the Science Mission Directorate (SMD) proved a key partner in steering HT-SSEP requirements development. GRC also sought input from Goddard Space Flight Center (GSFC) and Ames Research Center (ARC).

From conception, the SKEP project placed equal weight on the HT-SSEP needs expressed by domestic industry as it did NASA stakeholders. A weakness identified in past NASA electric propulsion developments has been a late request for industry end-user participation. While NASA often develops mission-enabling technologies, those technologies are typically transferred to industry at a TRL of 5 (demonstrated laboratory model) for further development and delivery of flight hardware. In theory, by doing so, NASA can become a marginal buyer of the technology with future availability of the technology driven by commercial demand, rather than ongoing NASA investment. However, the approach breaks down when NASA requirements overshadow industry needs and ultimately drive product cost beyond what is commercially viable. Also, when industry end-users are involved late in the development process, adequate engineering changes to support a successful commercialization may no longer be feasible within available schedule and budget. By involving industry early in the development process, the SKEP team sought to balance NASA and commercial needs to better ensure a product with a high likelihood of successful commercialization and future availability to NASA.

The project's original intent was to gather industry input through a request for information (RFI). This approach was abandoned early due to the burden an RFI can place on industry, especially when no request for proposal (RFP) is anticipated following the RFI. Industry feedback was ultimately sought through direct project team member participation in conferences and other public technical meetings. Specific attention was given to identifying spacecraft end-users, who could provide perspectives based on existing concepts for commercial small spacecraft. The input gathered from credible NASA and industry stakeholders provided the project with the needed direction to define the baseline concept and requirements.

III. Concept of Operations

In order for an HT-SSEP system to be successfully transferred to and commercialized by domestic industry, the unit cost of the HT-SSEP system must be commensurate with the cost of commercial small spacecraft buses. This necessity is a recurring consideration throughout the technology development. For this reason, prior to ATP, the decision was made that the HT-SSEP technology developed under the SKEP project would focus exclusively on a Hall-effect thruster based system. The two high maturity and performance electric propulsion technologies are gridded-ion and Hall-effect thrusters. Gridded-ion thrusters are compelling given their ability to achieve high propellant exhaust velocities, which minimizes a mission's total propellant mass requirement. By comparison, Hall-effect thrusters tend toward higher thrust, but lower exhaust velocities at similar power. The NASA Deep Space 1 and Dawn missions both utilized gridded-ion thrusters, resulting in the lowest mass spacecraft with the required propulsive capability. Lower spacecraft mass permits smaller launch vehicles, where the cost of the launch vehicle is often a major contributor to the overall mission cost.

That said, for low-cost small spacecraft, Hall-effect technologies are commonly believed to be the better alternative. Hall-effect thrusters are significantly less complex, thus less expensive to develop and fabricate, than gridded-ion thrusters of an equivalent power. The greater complexity of gridded-ion thrusters also translates to greater complexity and cost of the power processing unit (PPU). PPUs are often the most expensive element of an electric propulsion system, potentially many times the cost of the thruster. Furthermore, while very high propellant exhaust velocity is desirable for deep space missions, near-Earth missions tend to benefit more from higher thrust. Higher thrust shortens propulsion system operating time and travel time to destinations. For commercial missions, long transit times can result in significant loss of revenues. For national security missions, the ability to transit between orbits or otherwise maneuver rapidly is a tactical benefit. For NASA, the shortened transit time mitigates mission risk due to spacecraft health concerns, such as a decline in solar panel power generation, battery capacity, reliability of electronics, and structural integrity due to micro-meteorite impacts. While both gridded-ion and Hall-effect electric propulsion technologies provide NASA with important strategic capabilities, Hall-effect thruster based systems presently appear the stronger demand for small spacecraft electric propulsion.

Accepting that the HT-SSEP technology being developed under the SKEP project is focused exclusively on Hall-effect technology, the concept of operations consistent with stakeholder feedback is as follows. The propulsion system should:

- generate thrust by electrically ionizing and electrostatically accelerating propellant,
- neutralize the propellant ejected to prevent spacecraft charging,
- include the ability to reverse magnetic field polarity (to switch the direction of the swirl torque),
- protect the spacecraft against all conceivable propulsion system electrical faults,
- include thermal isolation between the thruster and spacecraft to limit spacecraft heating,
- accept an unregulated low-voltage power bus consistent with most small spacecraft,
- accept commands and return telemetry via a common small spacecraft communication protocol,

- require no on-orbit maintenance by the spacecraft other than survival heaters,
- satisfy testing as specified in the NASA GSFC General Environmental Verification Specification (GEVS) when no superseding requirement is recommended,
- operate at two qualified firing conditions, including nominal power and a reduced power state,
- operate at additional higher and lower than nominal power firing conditions (although they may not be fully qualified to minimize development cost), and
- employ a scalable, low-cost PPU architecture able to accommodate more than one domestic small spacecraft Hall-effect thruster (since a common PPU minimizes end-user development cost and minimizes mission risk in an environment where it remains unclear which thruster technologies will mature to flight).

Figure 1 is a block diagram depicting the interfaces between a small spacecraft and HT-SSEP device.

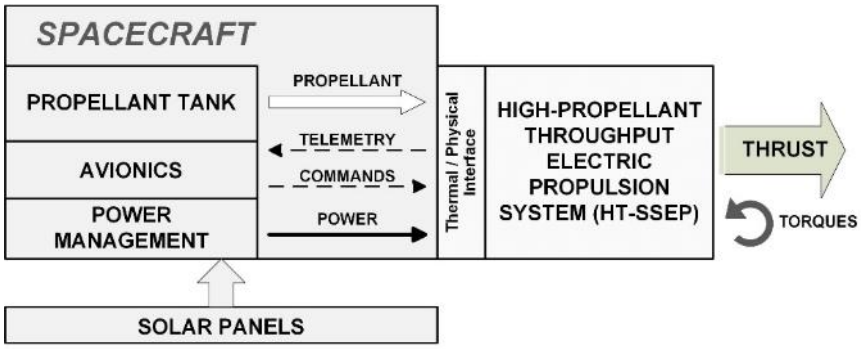

Figure 1: HT-SSEP propulsion system block diagram.

IV. Requirements

Thruster, PPU, and propellant feed system requirements were developed and vetted through discussion with stakeholders. For brevity, only select requirements are provided here in Table 1.

Table 1: Select HT-SSEP Requirements

Name	Requirement
Nominal Thrust	The propulsion system shall generate >= 40 mN of thrust at the nominal operating condition over its full operational lifetime.
Nominal Total Specific Impulse	The propulsion system total (anode + cathode flow) specific impulse shall be >= 1600 seconds at the nominal operating condition over its full operational lifetime.
Propellant Throughput	The propulsion system shall have a total propellant throughput capability of >= 100 kg at the nominal operating condition.
Propellant	The propulsion system shall meet all performance requirements when fed xenon propellant.
Cyclic Lifetime	The propulsion system shall be capable of 8,000 on/off cycles over its full operational lifetime.
Reversible Swirl Torque	The propulsion system shall have the ability to set the direction of the swirl torque induced by thruster operation.
Input Voltage	The propulsion system shall operate over an input voltage range of 24 to 34 VDC.
Enable Time	The propulsion system shall reach 95% of steady-state thrust in less than 10 seconds following receipt of the enable command.
PMA Outlet Pressure	The propulsion system shall meet all performance requirements when exposed to or operating at a pressure management assembly (PMA) outlet pressures of 40 +/- 3 psia.
System Mass	The propulsion system shall have a mass <= 10 kg (including thruster, PPU, flow controller, and interconnects, but excluding tank, gimbal, and PMA).

V. Architecture

A. Thruster Architecture

The thruster architectures considered were limited exclusively to those fitting the classification of Hall-effect. An architecture employing a center-mounted cathode was selected for its proven performance and packaging benefits. Electromagnets (rather than permanent magnets) were selected to allow for switching the direction of the magnetic field and in turn the induced swirl torque. This capability reduces the attitude control burden on the host spacecraft. An innovative magnetic field topology limiting discharge channel erosion was selected to achieve the performance and propellant throughput requirements. A cathode employing a swaged heater for conditioning was baselined (rather than a heaterless cathode) based on the project's preference towards high-TRL technologies wherever possible to limit development risk as well as to avoid imposing additional complexity on the PPU and feed system architectures.

B. PPU Architecture

Development of the PPU architecture was driven largely by three desired attributes. First, the architecture should be sufficiently scalable and flexible to permit operation of more than one domestic low-power Hall-effect thruster. Thrusters considered in the trade space included the NASA-H64M, NASA-H71M (under-development), JPL MaSMi-DM, Busek BHT-600, Busek BHT-200, and Apollo Fusion ACE. Compatibility of any thruster was not required if determined that a significant increase in PPU cost was anticipated. Second, the architecture should favor simplicity (i.e. recurring unit cost) over performance. Third, the architecture should favor approaches minimizing current and future development costs. Note that minimizing current development cost of a PPU favors solutions familiar to the development team. The architecture described here is believed appropriate for small spacecraft and readily achievable given the particular knowledge and experience of the SKEP PPU development team. Other low-power PPU implementations may be equally worthy and preferred by other development teams. The chosen PPU architecture for further development by GRC is shown in Figure 2.

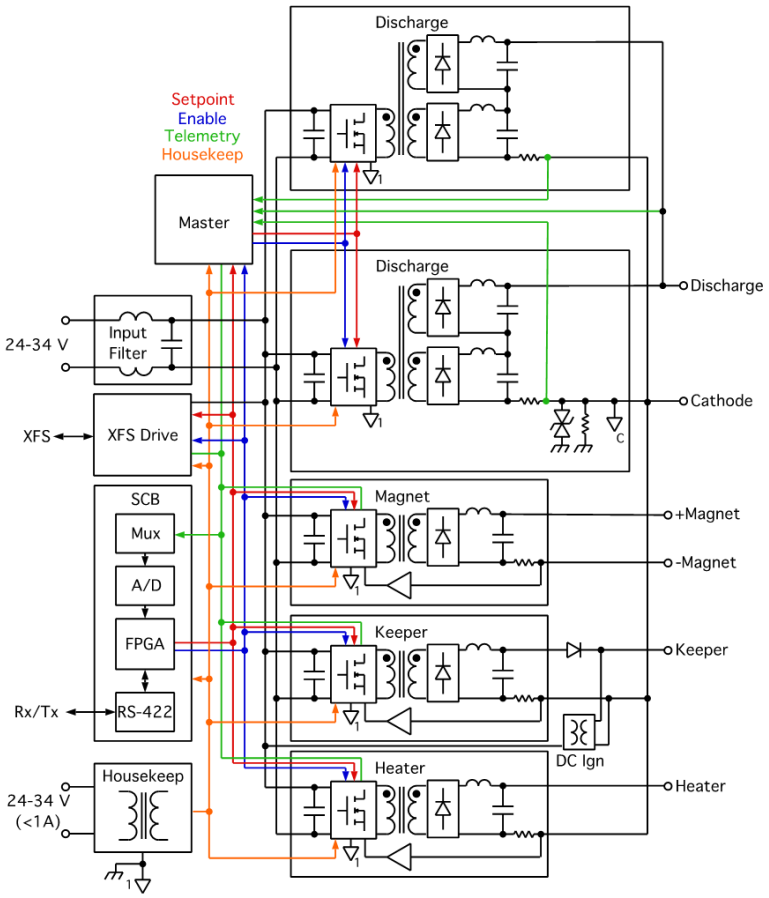

Figure 2: Scalable common PPU architecture for low-power small spacecraft.

The PPU conceptually consists of four or more “slices”, where each slice is an independent board within the unit. The PPU conceptually includes:

- a slice for the system control board (SCB),
- a slice for auxiliary power supplies to operate the electromagnets, cathode keeper, and cathode heater,
- a slice for housekeeping, flow control driver, input filter, and other miscellaneous functions, and
- one or more slices for parallel scaling of the discharge power supply.

By design, a single discharge module could power the Busek BHT-200 or Apollo Fusion ACE. Two discharge modules could power the NASA-H64M, NASA-H71M, JPL MaSMi-DM, or Busek BHT-600 at their nominal operating conditions. Three discharge modules could provide excess capacity to operate the thrusters at higher than nominal operating conditions or to provide redundancy.

Parallel discharge power modules offer numerous benefits. The approach not only enables scaling to accommodate the thrusters considered, but also supports higher power thrusters not yet considered, thus minimizing future development costs to the end-user. Splitting the load between modules reduces component stress compared to a single higher-power module. This is especially true given the high-voltage transformer step-up ratio required and the low-voltage bus input. While not a design driver, the approach further provides improved electrical efficiency compared to a single module. Other benefits include the ability to stagger switching to reduce current ripple or disable/enable modules as operating conditions change to optimize efficiency. Drawbacks of the multi-module discharge power supply are higher parts count, mass, and cost than a single module. Additionally, multiple discharge modules require a master controller to manage current sharing, although this can easily be integrated within one of the discharge modules. The PPU design team’s conclusion was that the multi-module discharge supply provided the simplest approach to satisfy the stakeholder need for scalability, without developing and maintaining a costly product line of different power PPUs.

The discharge module rectifiers are conceived as two in series. The series rectifiers reduce output voltage component stress compared to a single rectifier stage. Additional rectifier stages can be added for higher output voltage, although electrical efficiency declines and parts count increases with each stage. Higher voltage components may also be implemented than considered for this architecture to limit the number of stages. The de-rated voltage limit of the components notionally considered were selected due to their common spaceflight availability. The availability of spaceflight components decreases with higher voltage requirements, where in the worst case only a single spaceflight-qualified component may exist. Components of rare availability were avoided during the PPU development to mitigate the impact of component obsolescence.

The discharge module pulse-width-modulation circuit includes both discharge voltage and current regulation loops (i.e., current limit) to prevent damage to the thruster during faults and to enable glow-mode thruster startup. The approach has heritage to previous PPU designs, allowing GRC to leverage proven circuitry.

In order to minimize parts count and cost, the auxiliary supplies were conceived to utilize the same power converter topology, requiring only minor differences to account for discrepancies in each auxiliary’s power requirements. The auxiliary supplies for the cathode keeper and heater require isolation given they float at cathode potential. Although the thruster electromagnets are electrically isolated, it is NASA’s best practice to utilize an isolated supply to protect against a potential short to thruster body. An important complication of the common auxiliary topology approach is the challenge of meeting the high-voltage output requirements for keeper ignition at end-of-life. While many high-power PPUs employ a separate pulsed ignitor, the GRC-heritage pulsed-ignitor design does not fit the expected cost and form factor for a low-cost small spacecraft PPU. Rather, the PPU development team settled on following common laboratory practice of a DC ignitor, far more compact and requiring many fewer components compared to the GRC-heritage pulsed ignitors.

The SCB receives propulsion commands from and sends telemetry to the spacecraft. The SCB executes programmed control sequences for the electric propulsion string, sets each power module operating condition, enables power modules at the required intervals, regulates propellant flow rate, senses for fault conditions, and disables the thruster when necessary. A Field Programmable Gate Array (FPGA) is a good compromise between programming functionality, complexity, and cost. An FPGA has become the preferred choice for PPU programmable logic, although microprocessors and discrete-circuit state machines have been used in the past.

Figure 3 shows conceptually how a dual-discharge module configuration might be implemented. The smallest blocks shown represent the discharge and auxiliary module MOSFETs. The larger blocks shown conceptually represent the magnetics. Given the heat dissipation requirements for these components, they would notionally be located near the base of the PPU for efficient heat sinking to a cold plate.

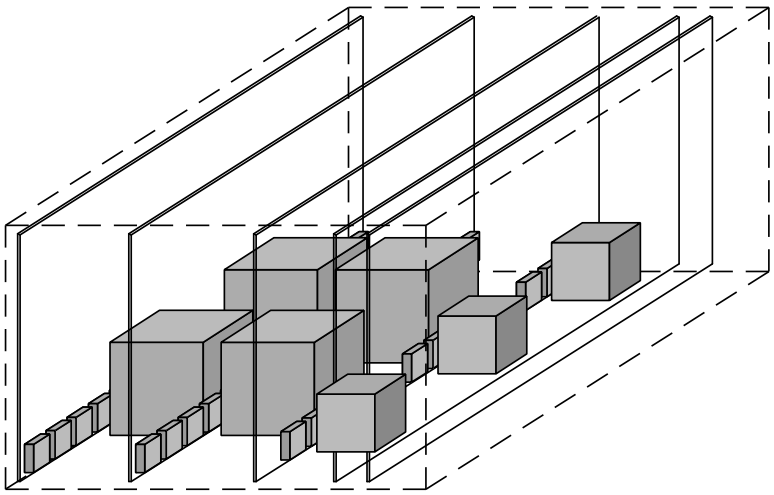

Figure 3: PPU packaging concept.

C. Propellant Feed System Architecture

For the purpose of HT-SSEP early development, a laboratory feed system was implemented. However, to develop adequate thruster and PPU requirements, the flight feed system architecture needed to be considered. Various configurations were traded. At one end of the spectrum, the feed system team considered a xenon flow control module (XFCM) providing only binary states. For example, given the fixed output pressure of the PMA, a feed system can be implemented with low-cost flow restrictors and latch valves where only one or two flow conditions are permitted. The key benefit to such an approach is low cost. Drawbacks include considerable variability in the nominal mass flow between units based on manufacturing tolerances. Furthermore, mass flow rate can vary with changes in environmental conditions. On the other end of the spectrum, the team considered heritage GRC XFCM assemblies and those baselined for future use on high-power SEP systems. While these feed systems offer considerable capability and often redundancy, their cost, size, and complexity substantially exceed the needs of the average NASA/industry small spacecraft mission considered.

The development team's preferred concept for the HT-SSEP feed system architecture fell somewhere in between and is shown in Figure 4. The wide operating range of the thruster can be accessed by regulating a single proportional control valve (PFCV). While ideally both the anode and cathode would have independent PFCVs to optimize performance, the added complexity was not justifiable for a low-cost small spacecraft. Furthermore, a separate PFCV on the cathode line may necessitate the added complexity and cost of a cathode pressure sensor to support feedback control. Whereas, the anode flow rate can be reliably regulated based on the discharge current once the thruster is operational. Since discharge current monitoring exists in the PPU by default, no additional sensing is required. The least complex solution to provide the cathode with a known flow rate is use of flow restrictors to split propellant supply to the cathode at between 5-10% of the anode flow rate. While conceptually simple, the approach does have some drawbacks. Matching precision orifices or other flow restricting devices to provide the desired flow fractions to both the anode and cathode comes with some uncertainty. As such, the cathode flow fraction needs to be set conservatively rich (closer to 10% than 5%). This reduces the effective specific impulse of the propulsion system. Also, the cathode flow fraction cannot be optimized on orbit depending on the desired operating condition. Since small spacecraft are anticipated to operate primarily at only one or two operating conditions over their lifetime, limiting the ability to optimize the cathode flow fraction seems reasonable. The flow fraction would be optimized for the HT-SSEP system's nominal operating condition, while ensuring acceptable operating behavior at off-nominal conditions. A small decrease in total specific impulse was determined a reasonable trade to limit cost, complexity, mass, and packaging envelope of the feed system.

It is also anticipated that the PFCV is a normally-closed valve and doubles as an isolation valve. The PMA is anticipated to provide at least two additional isolation valves, controlled by the spacecraft, in series to protect against leakage. The XFCM would also include a survival heater to be regulated by the spacecraft or the XFCM installed in a spacecraft location to benefit from existing spacecraft thermal controls.

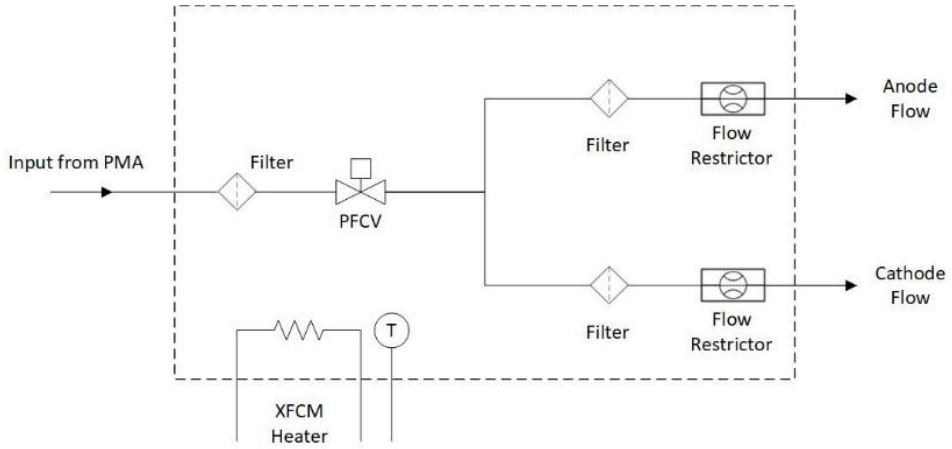

Figure 4: Feed system architecture concept.

VI. Hardware Component Development

A. Magnetic Circuit Development

The NASA-H64M thruster's innovative magnetic field topology was designed and simulated in a commercially available magnetics modeling software to provide characteristics found in recent NASA developments necessary to achieve high thruster performance with high-propellant throughput capability. At the same time, the field topology was optimized for a small spacecraft thruster design, which has some differing development challenges from its high-power counterparts. While the initial magnetic circuit simulations were performed using a 2-D model of the thruster to define rough geometries, the final detailed magnetic circuit simulations utilized a full 3-D CAD model consistent with all thruster features as represented in manufacturing drawings.

Extensive and detailed experimental magnetic field mapping of the assembled magnetic circuit was performed. Two dimensional and linear maps were performed at various thruster magnetic current settings. Mapping results showed excellent agreement with magnetic simulation predictions (both 2-D streamline and linear maps along discharge channel centerline). For example, in Figure 5, the thruster's normalized measured channel centerline magnetic field profile at various azimuthal locations proves to be axisymmetric (as predicted by the magnetic simulation). The profile shown in Figure 5 resulted in the desired thruster performance. A short-duration wear test also confirmed the design intent to achieve limited erosion of the discharge channel and propellant distributor.

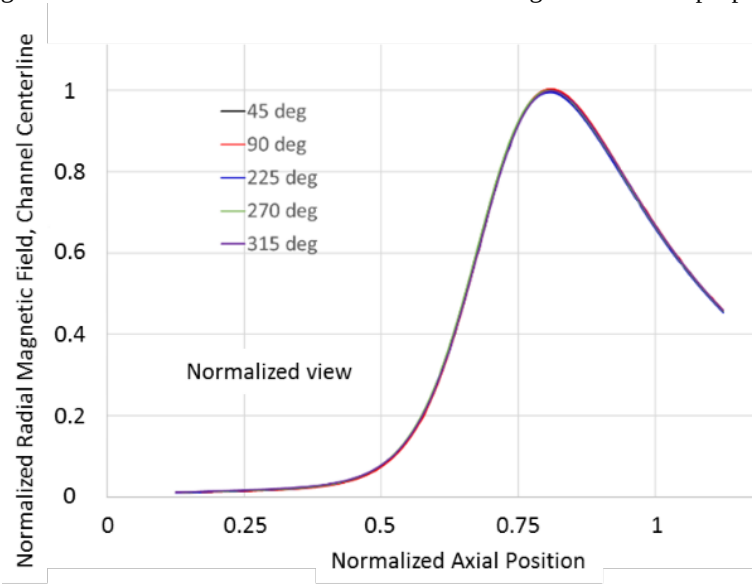

Figure 5: Channel centerline magnetic mapping results at various azimuthal angles for the NASA-H64M-LM thruster.

B. Propellant Distributor Development

Ensuring azimuthal neutral flow uniformity in a Hall-effect thruster's channel downstream of the propellant distributor is critical to achieving high thruster efficiencies, minimizing discharge instabilities, and avoiding plume asymmetries [5] [6]. The common approach is integrating the propellant distributor with the discharge anode. A variant of a GRC-heritage design [7] with minor innovations was developed for the NASA-H64M. The propellant distributor maintained the key features of the heritage design providing excellent flow uniformity, but made incremental changes to better meet the lower-cost goals for small spacecraft.

Gas flow simulations provided important insight during the anode development. The propellant flow in the upstream portion of the distributor can be effectively described by laminar viscous flow relations and is designed to evenly distribute flow from the inlet around the circumference of the annulus. The effects of flow restrictor variances based on manufacturing tolerances around the anode affect the upstream pressure distribution, and the analysis is iterated to converge on a consistent solution. Monte Carlo type procedures were applied to examine the resultant statistical distribution and assess various preliminary manifold designs for their robustness to manufacturing variances and ability to maintain sufficient flow uniformity.

The downstream portion of the distributor, including exit flow into and out of the discharge channel, is in the transitional and rarefied flow regimes and was modeled via a direct simulation Monte Carlo (DSMC) code. Again, multiple preliminary designs and variants were examined to evaluate their ability to provide sufficiently uniform flow that is robust to potential flow and manufacturing variances. Figure 6 illustrates a sample set of discharge channel flow uniformity simulation results that highlight how modest differences in propellant distributor design, including again effects of deviation from various manufacturing tolerances, can lead to substantially differing performance. These gas flow simulations provided important insights informing key propellant distributor design decisions.

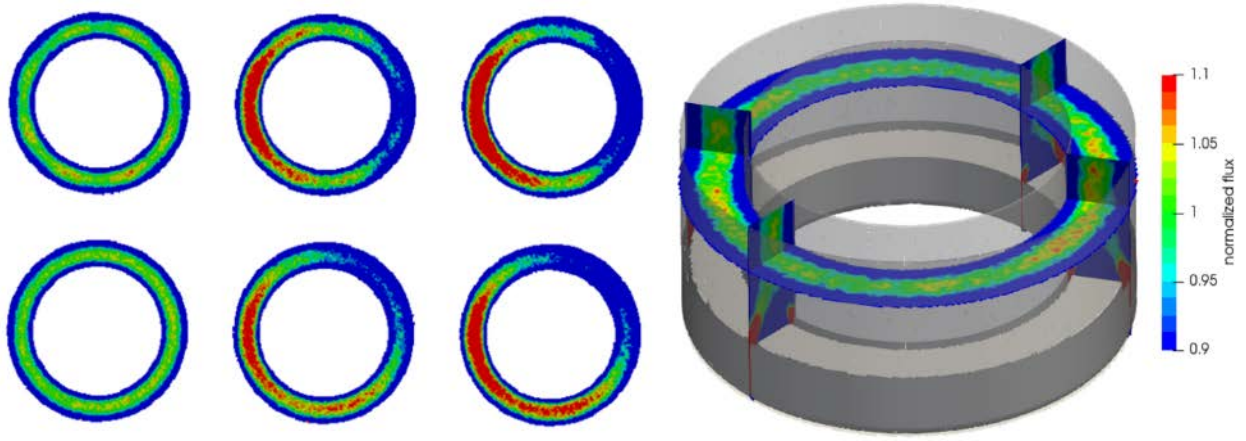

Figure 6: Sample discharge channel flow uniformity simulation results. (Left) 2-D flux distributions for various design implementations. (Right) 3-D flux distribution for a single design implementation.

Following propellant distributor manufacturing, experimental flow characterization was conducted in GRC's VF-8 vacuum test facility. The distributor was mounted in an aluminum housing geometrically identical to the NASA-H64M-LM's ceramic discharge channel. The facility background pressure was approximately 2 μTorr, while xenon propellant was fed into the propellant distributor's inlet at rates ranging from 10 to 30 sccm. Downstream of the propellant distributor's plasma-facing surface, a pressure transducer mounted on a 4-axis motorized stage made measurements at 11.25° azimuthal angular increments. At each azimuthal angle, nine data points were acquired at the locations as indicated in Figure 7. These locations spanned radially from the inner to the outer channel walls and axially from the mid-channel to the thruster exit plane.

Figure 7 also shows a representative example of the flow uniformity experimental characterization results overlaid on the theoretical prediction. The normalized pressure transducer data for the mid-channel, channel-centerline location is shown for a xenon flow rate of 25 sccm. Both the simulation and test data indicate excellent azimuthal neutral flow uniformity to within ±5%.

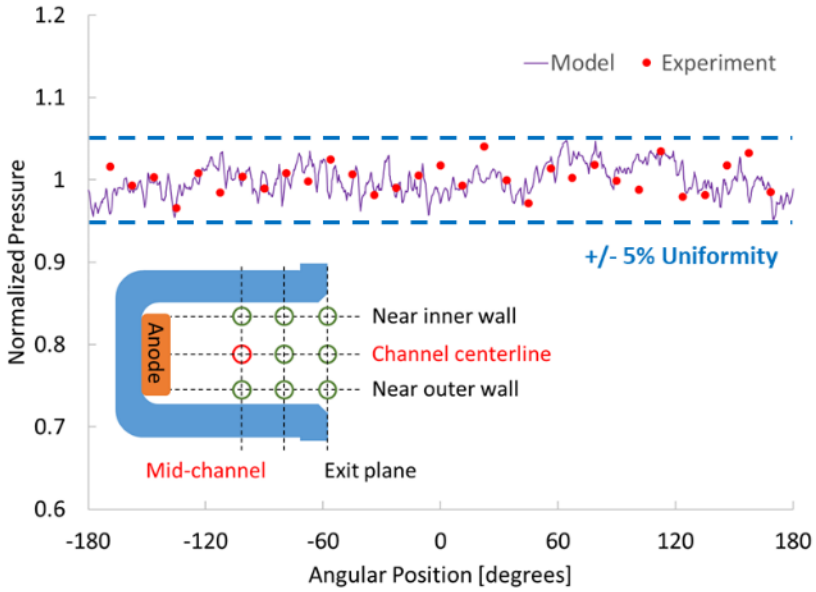

Figure 7: Azimuthal neutral flow uniformity results at the mid-channel, channel-centerline location for the NASA-H64M-LM propellant distributor operating with a 25-sccm xenon flow.

C. Low-Current Hollow Cathode Assembly Development

The GRC-heritage cathode assembly, illustrated in Figure 8, consists of six primary components broken down by function: a) the refractory metal tube and orifice plate which contain the emitter and maintain a relatively high local pressure during propellant flow; b) the low-work function emitter which generates the charged particles to efficiently maintain a plasma inside the cathode; c) the swaged heater and the radiation shield provide heating of the emitter during conditioning and ignition processes; and d) the keeper, which is used to ignite the discharge within the cathode, support low current cathode operation, and protect orifice plate from particle bombardment during primary discharge operation.

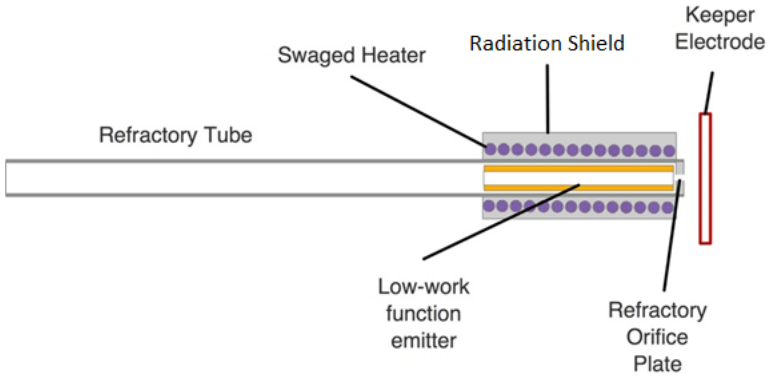

Figure 8: Illustration of cathode developed for H64M thruster.

This type of hollow cathode has been used in many types of electric propulsion. GRC's use of these devices include:

1. the International Space Station (ISS) Plasma Contactor Units (PCU) where GRC engineers designed, manufactured, tested, and delivered the hollow cathode assemblies,
2. NASA missions Deep Space 1 and Dawn employed cathodes based on the ISS PCU design as part of the successful use of gridded-ion engines for primary propulsion, and
3. the NEXT Ion Engine [8] and AEPS Hall thrusters both use hollow cathodes whose designs evolved from the previous programs and employed many of the same processes for cathode fabrication and use.

The NASA-H64M cathode assembly maintains these heritage design approaches wherever possible, although some allowances were made for the unique packaging requirements.

To operate nominally over the range of 1 to 3 amps emission current with an anticipated lifetime in excess of 10,000 hours, the hollow cathode design was scaled from prior instances in order to meet the necessary thermal requirements for efficient plasma production. Building off prior work on small cathodes [9] [10] [11], the cathode was sized to ensure the cathode reached the required temperatures as well as fit within the volume allocation within the H64M thruster. The cathode tube and orifice dimensions were scaled based on lessons from the prior work to ensure the emitter temperature reached the nominal operating temperature of 1050 C [12] and maintain a sufficiently high internal pressure.

Once cathode assemblies were fabricated, they underwent testing in GRC's VF-56 vacuum test facility. These tests determined the appropriate heater operating conditions for cathode conditioning and ignition, demonstrated diode and triode mode operation to the keeper and an external anode respectively, and characterizing plume-mode transition behavior. Additionally, cathode temperature measurements were made via thermocouples and optical pyrometry. Figure 9 shows representative data from the first fabricated cathode installed in the H64M indicating discharge voltage as function of emission current and xenon flow rate. The results are in line with expectations based on prior GRC cathode development work.

An alternative approach that exists for power-restricted thruster systems is to use a heaterless hollow cathode. Rather than initiating thermionic electron emission by pre-heating the cathode emitter with a swaged heater, the PPU raises the keeper voltage until a Paschen breakdown occurs. As the cathode self-heats, the emitter transitions to thermionic emission for cathode operation. Heaterless cathodes, in principle, resolve a potential risk by eliminating the need for the swaged heater of heritage devices that requires burdensome process control. While heaterless cathodes have been used in industrial processes where maintenance can be accommodated, they are still considered low TRL for spaceflight application because the approach has not been validated in ground life testing or space use. Additionally, the heaterless cathode startup can place an increased burden on the complexity of the PPU and propellant feed system design [13]. Thus, the operational benefits by implementing a heaterless cathode need to be carefully assessed against other system impacts to complexity and cost.

A more tangible advantage of the heaterless cathode is its packaging benefits. For small thrusters, removing the cathode heater provides an attractive relaxation of design limitations for center-mount cathodes. With heaterless cathodes, Hall-effect thrusters with center-mount cathodes can in theory get smaller than exemplified by the NASA-H64M-LM. That said, at the scale of the H64M, a largely heritage cathode with swaged heater has been demonstrated to package acceptably. As such, given the project preference towards heritage technologies for this development, the swaged heater approach was baselined.

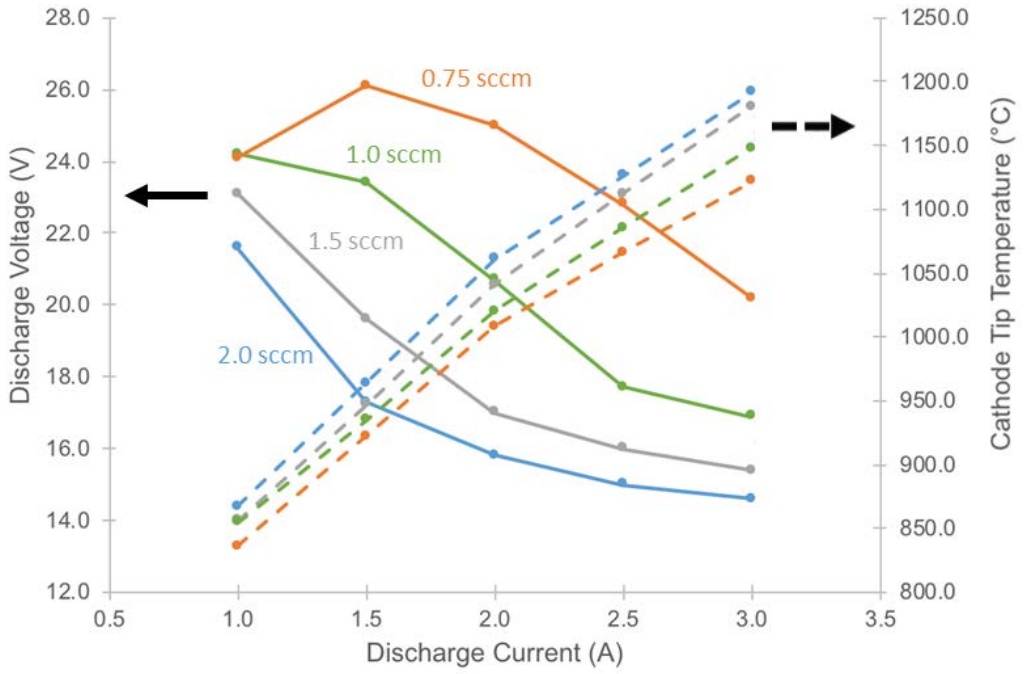

Figure 9: Hollow cathode diode-mode characterization as a function of xenon flow rate.

D. PPU Discharge Power Supply (DPS) Breadboard Development

The discharge power supply (DPS) produces the high voltage necessary to accelerate the thrust-generating plasma. In doing so, the DPS processes up to 95% of the PPU's total power. As a consequence, the DPS is a key driver of the overall PPU mass, volume, electrical efficiency, scalability, and cost. Proportional to its importance, much of the PPU development to date has focused on the DPS, including:

- trades between prospective DPS power converter topologies,
- simulations in commercially available electronic circuit modeling software,
- commercial-off-the-shelf (COTS) parts selection with spaceflight equivalents,
- prototyping using solderless breadboards,
- development of custom magnetics in cases where COTS magnetics were deemed inadequate,
- production of breadboard printed circuit assemblies (PCA),
- benchtop circuit testing using passive load banks, and
- integrated testing using an active plasma source.

For the sake of brevity, the full details of the discharge supply development will not be reviewed here. These details are anticipated in a future publication. With regard to the discharge supply development, this paper will focus on the selected topology, general attributes of the design, and measured power processing efficiency.

Developing a Hall-effect thruster DPS intended for small spacecraft applications has challenges less common to the GRC-heritage, multiple-kilowatt DPS. Notably, small spacecraft buses commonly provide only low-voltage, unregulated 28-V power to payloads, including propulsion. In contrast, GRC-heritage discharge supplies receive both low- and high-voltage inputs from the spacecraft bus, with low-voltage input for PPU controls and high-voltage input to the DPS. So for small spacecraft buses, the low-voltage input to the DPS results in very high primary currents even for a sub-kW converter. For example, a DPS consuming 1 kW of power will draw 42 A of current when the bus voltage falls to 24 V. Managing the conduction losses in the primary side of the converter thus becomes paramount to maintaining efficiency and minimizing component heating. In addition, the Hall-effect thrusters considered in this development require voltage outputs of 250 to 350 V to operate at nominal conditions. This creates the need for a converter with a large transformer step-up ratio to boost the input voltage enough for proper thruster operation. Finally, size, weight, and cost must be carefully managed at this power level to remain commensurate with the needs of small spacecraft. Size, weight, thermal management, electrical efficiency, and cost must be continuously and carefully traded with every design decision.

The development process began by conducting a trade study to determine suitable topologies for the DPS. Simulations were conducted to provide a rough estimate of efficiencies and performances of the topologies considered. Early simulation results favored two topologies, the Weinberg converter and the full-bridge. Both topologies were experimentally evaluated in the desired power range with solderless breadboard assemblies. Although both converters have compelling strengths and weaknesses, the GRC development team ultimately selected the full-bridge for continued development. The development team observed better early success achieving the desired performance with the full-bridge circuitry. This outcome may well be the result of GRC's more extensive experience with constructing full-bridge discharge converters as used in heritage designs. The selection of a full-bridge for this development should not be considered conclusive of the topology's superiority for the given application. Rather, the topology selected reflects the project's preference towards minimizing development risk. The selection is further solidified by the development team's modestly superior results with the full-bridge prototype breadboard.

The full-bridge DPS operates from an input voltage of 24 to 34 VDC to be compatible with the anticipated small spacecraft's 28-V unregulated power systems. A DPS breadboard module was designed, and two iterations of PCA were fabricated. Each iteration from the original solderless breadboard made incremental improvements and added additional capability. The DPS as presently baselined has a capability of processing up to 375 W of power and a voltage output up to 350 VDC. Two or more DPS modules can be operated in parallel to scale the discharge power, with three modules in parallel thus far demonstrated. Output voltage and current regulation controls allow for any of the common thruster start-up modes (i.e., hard, soft, or glow-discharge).

The full-bridge topology operates at a switching frequency 50 kHz and uses a custom lightweight foil transformer design. The transformer has a single foil-wound primary and two secondary windings. Current is shared by parallel drive MOSFETs with a single driver for each high-low pair. Full-wave rectifiers are used on each secondary with series-stacked L-C output filters, and snubbers provide peak diode voltage limiting. The output inductor was similarly custom designed for improved performance. Bulk capacitance across the output supports normal thruster oscillations. The single module efficiency, including all improvements to date, is 92-95% across the full design power and input bus voltage range (Figure 10).

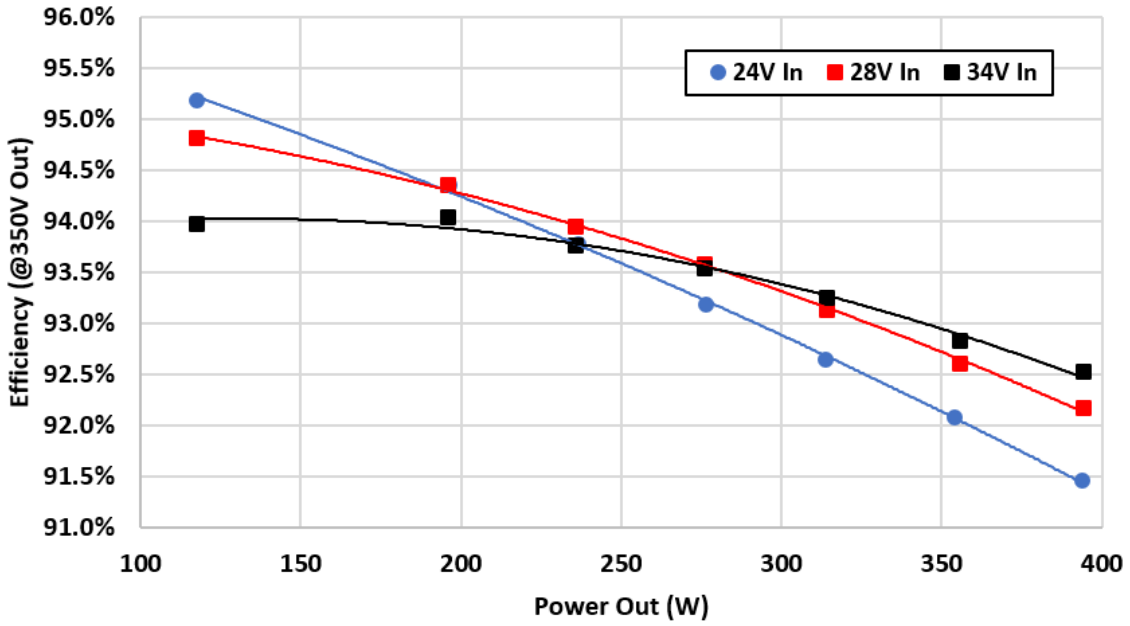

Figure 10: Single DPS module efficiency versus power at 350-V output condition for 24-V, 28-V, and 34-V input.

Following successful demonstration of a single DPS, two additional DPS modules were populated (including a master controller) and connected in a parallel-output configuration, shown in Figure 11. They were subjected to comprehensive performance and functional testing including efficiency, regulation, transient response, and loop stability. The three modules together had similar performance to the single module setup, but further improvement is anticipated. When the three-module results in Figure 12 were recorded, only one of the three boards included all improvements to date. Specifically, two of the modules used COTS input filter inductors, rather than a custom inductor design. Regardless, the three-module configuration at lower power output demonstrates low system power loss that is acceptable over the full design operational range.

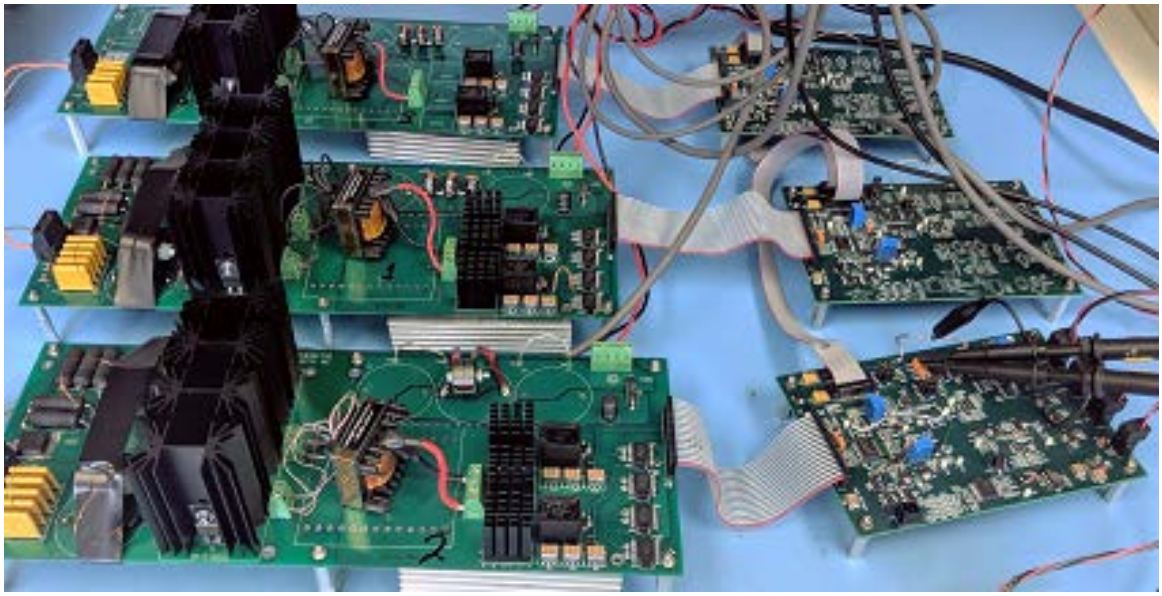

Figure 11: Three-module breadboard discharge power supply; layout to be optimized for parts density in future iterations.

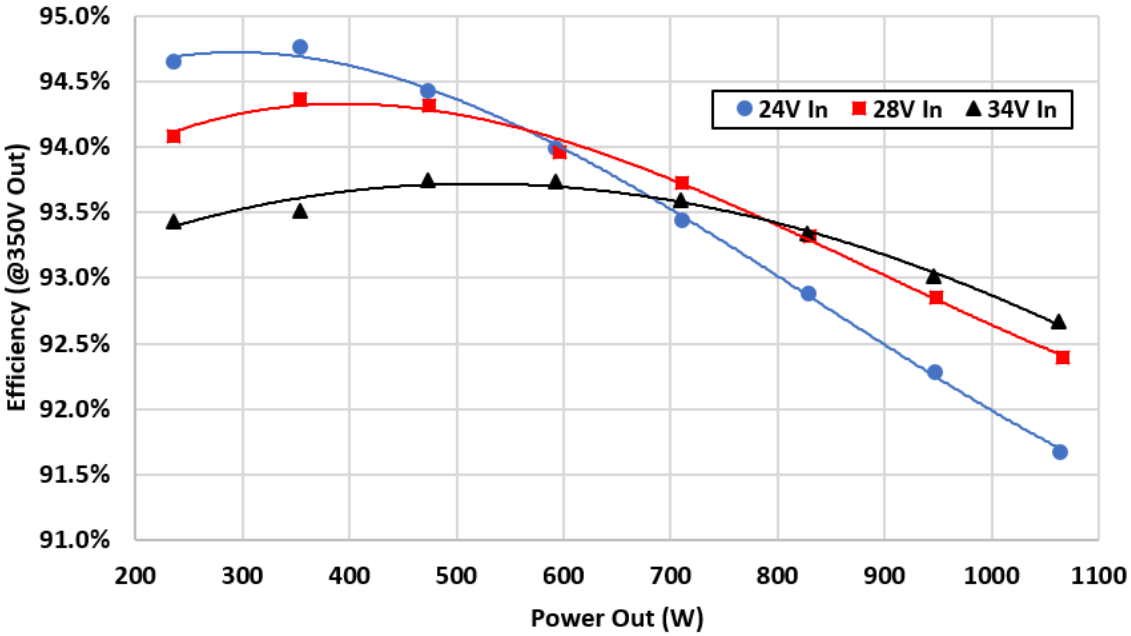

Figure 12: Three DPS module efficiency versus power at 350-V output condition for 24-V, 28-V, and 34-V input.

E. PPU Auxiliary Module Breadboard Development

The PPU further requires auxiliary supplies that provide power for the thruster's electromagnets, cathode heater, and cathode keeper. A flyback topology was selected for its simplicity and its ability to meet requirements for all three auxiliary power supplies. The converter can be configured to output modestly high voltages (~150 V) desirable during cathode keeper ignition or configured for the lower voltages necessary to power the electromagnets and cathode heater (~10 V). The flyback topology offers the necessary isolation between the input and output. Use of a common topology between the three auxiliaries will minimize the development and recurring unit cost. Enforcing a common topology may result in lower auxiliary supply electrical efficiencies than otherwise achievable, but given that the DPS dominates power consumption by an order of magnitude, inefficiencies in the auxiliary supplies have minimal impact on the overall PPU electrical efficiency. A switching frequency of 100 kHz was selected for mass and volume reductions.
As a proof-of-concept, a cathode keeper supply was designed, built, and demonstrated as first a solderless breadboard and then PCA. Although the auxiliaries will eventually be nearly identical, the most challenging of the three applications is the cathode keeper power supply with its higher output voltage requirement. While typical keeper supply operation draws about 5 W, the keeper supply is required to output 30 W at up to 40 V and 1 A steady-state. As with the DPS, the input voltage range is 24 to 34 VDC. During cathode keeper ignition, a zero-load voltage in excess of 100 V was targeted. The minimum efficiency and output current ripple targets were 80% and 5%, respectively.

Once fabricated, extensive benchtop testing on a resistive load was performed. An example dataset is provided in Table 2. Data was recorded for the maximum current output of 1 A and the two voltage output conditions of 15 and 30 V for input voltages of 24, 29, and 34 V. In all instances, the calculated efficiency is about 80 percent.
Considerable room for improvement still remains with the cathode keeper breadboard, so the calculated efficiency should be considered a lower bound.

Following benchtop testing, the breadboard cathode keeper supply was tested with a low-power cathode in GRC's VF-56 vacuum test facility. The test demonstrated repeated cathode ignitions and steady state operation. Operating range was demonstrated with output currents ranging from 0.3 to 1 A.

Table 2: Cathode keeper breadboard benchtop testing on a resistive load.

Load [Ohms]	V_{in} [V]	Power [W]	I_{out} [A]	Efficiency
15.2	24	19.3	1.0	78.8%
15.2	29	19.1	1.0	79.6%
15.2	34	19.1	1.0	79.6%
30.1	24	37.5	1.0	80.3%
30.1	29	37.2	1.0	80.9%
30.1	34	37.0	1.0	81.4%

F. PPU Keeper Ignitor Breadboard Development

The cathode keeper at beginning of life often requires little more than 30 V to reliably ignite the cathode. However, as the cathode ages, cathode ignition may require noticeably higher voltage. Using a flyback converter for the cathode keeper supply, well over 100 V can easily be achieved at no load, which provides significant margin. Even so, heritage GRC designs have utilized 600 V pulsed to guarantee cathode ignition across the propulsion system's lifetime and exposure to a range of environments.

While the GRC-heritage, high-voltage pulsed ignitor is relatively large, complex, and costly to achieve the desired pulse characteristics, these properties are rather modest compared to the overall size, complexity and cost of a PPU for moderate to high-power applications. If however applied to a low-power PPU, the heritage pulsed ignitor fails to scale appropriately and becomes a disproportionate contributor to the low-power PPU's size and cost. The two prevailing paths forward were to either attempt development of a new pulsed ignitor for low-power needs based on a different topology than the heritage PPUs, or to simplify the requirements. The project ultimately decided that the most appropriate approach was a high-voltage DC ignitor. A high-voltage DC ignitor is a very simple, compact, and low-cost circuit consistent with the needs of small spacecraft. While a DC ignition may be marginally less reliable than a pulsed ignition, it is the common cathode ignition approach in laboratory settings with demonstrated reliability as long as the cathode emitter is handled in accordance with documented handling and conditioning procedures.

The cathode keeper ignitor is configured in parallel with the cathode keeper supply, ramping to a maximum of 600 V until cathode ignition is achieved. A blocking diode protects the cathode keeper supply output from the DC ignitor high voltage as shown in Figure 13.

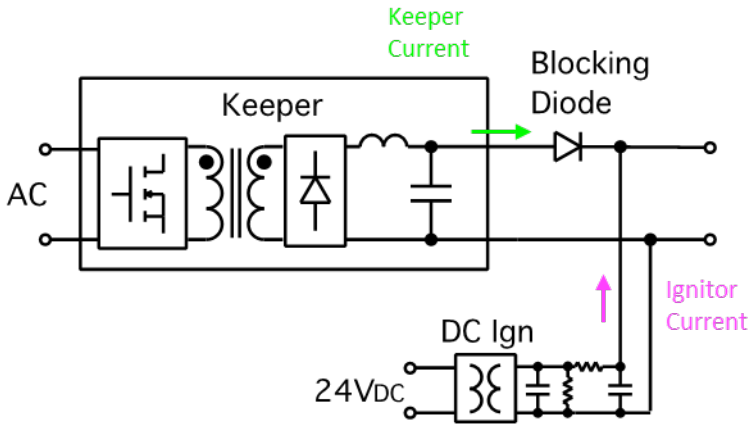

Figure 13: Schematic of cathode keeper ignitor configured in parallel with the cathode keeper supply output.

The proof-of-concept breadboard ignitor was built with a COTS high-voltage DC-DC supply. The DC-DC supply is a high-reliability part tested per MIL-STD-883. However, the path-to-flight for this COTS part is uncertain. Once constructed in a breadboard, the ignitor was evaluated using an 1/8" low-power laboratory cathode in GRC's VF-56 vacuum test facility. Once the cathode heater reached ignition temperatures, the cathode keeper supply was activated to 22 V, a voltage known to be too low to ignite the cathode but high enough to maintain the cathode if ignition was achieved. Activating the 2-mA ignitor circuit caused the keeper output voltage to increase until approximately 30 V was exceeded, and ignition successfully occurred with the operational voltage dropping to approximately 21 volts. The ignition sequence was repeated several times to verify consistent operational behavior. Figure 14 shows a characteristic oscilloscope trace with the ignition behavior described.

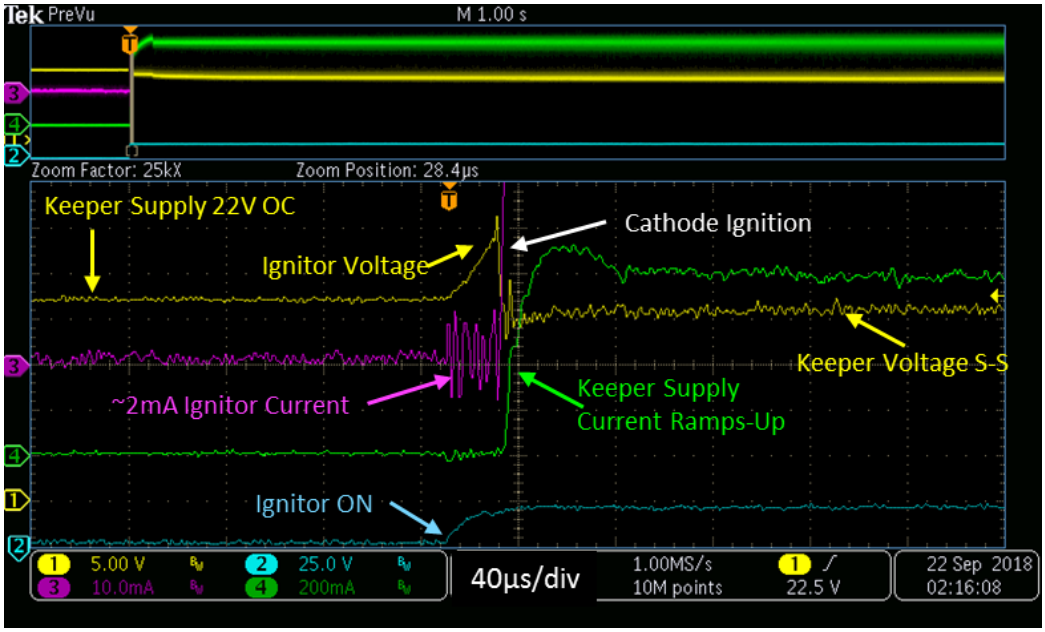

Figure 14: Characteristic oscilloscope trace from cathode ignition demonstration using an 1/8" low-power cathode in GRC's VF-56 with a breadboard ignitor based on COTS components.

Since the hot cathode required only a minimal increase in voltage to initiate the plasma, the test was repeated with a cold cathode to make sure the ignitor was capable of achieving high voltages. While connected to the laboratory data acquisition system (DAQ), the ignitor supplied a peak of 460 V to the cathode keeper. Disconnecting the DAQ, which included a voltage divider resulting in parasitic loss, the expected 600 V was demonstrated.

Given concerns regarding the COTS DC-DC converter's path-to-flight, a custom high-voltage DC ignitor supply was designed using a push-pull circuit with a voltage multiplier, as seen in Figure 15. The circuit can easily generate high voltages from the nominal 28-V input and scale to higher voltages by adjusting transformer turns ratio or adding multiplier stages. The proof-of-concept used open-loop, unregulated operation for simplicity. The transformer minimum size was limited by in-house magnetics fabrication capability. A 100-kHz switching frequency was implemented in the same manner as the auxiliary supplies, although higher frequency can further reduce the circuit size. Figure 16 provides an exemple waveform from testing of the proof-of-concept, custom high-voltage DC ignitor supply. As configured, the ignitor generated ~375 V from a 20-V input. The ignitor will be further refined and included in the next cathode keeper supply PCA.

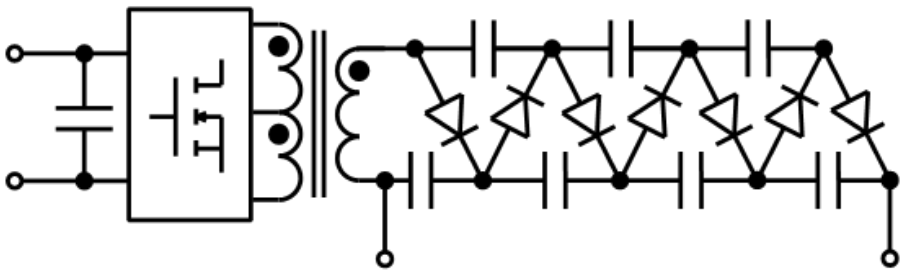

Figure 15: Schematic of keeper voltage multiplier ignitor.

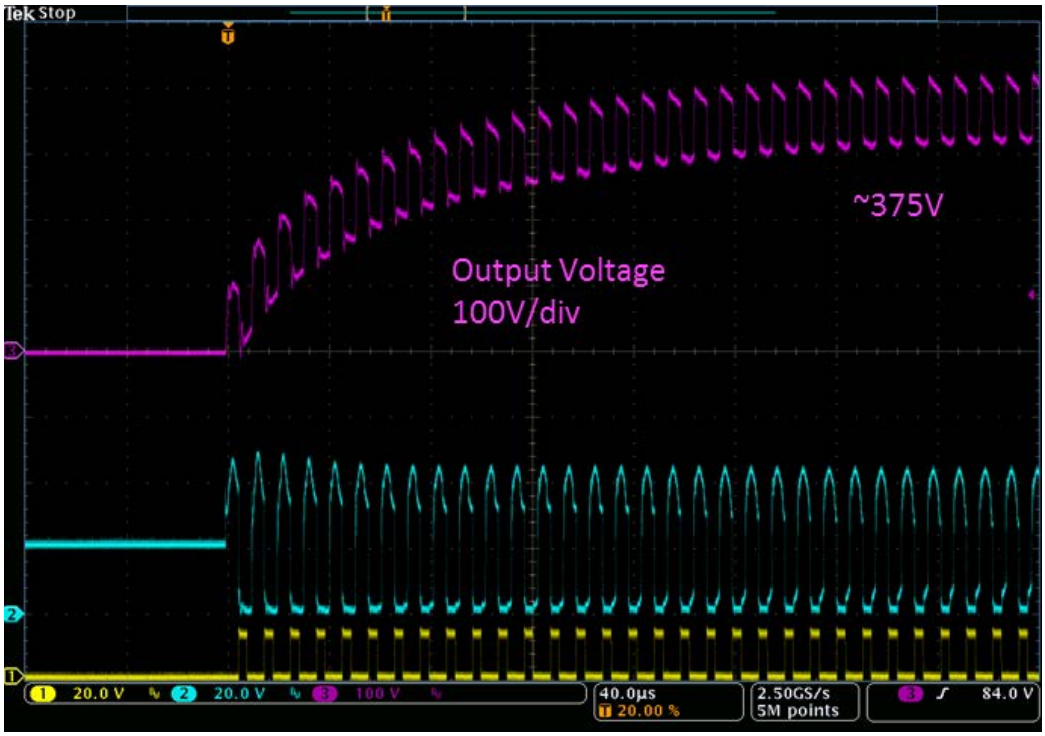

Figure 16: Sample waveform from benchtop testing of a proof-of-concept, custom high-voltage DC ignitor supply with path-to-flight.

VII. NASA-H64M-LM Thruster Test Results

Performance, stability, wear, and thermal characterization was conducted on the NASA-H64M-LM to demonstrate the design's viability for supporting small spacecraft propulsive needs. A wider-channel modification (15% wider) of the NASA-H64M-LM thruster, referred to herein as the NASA-H64M-LMW, also underwent performance and stability characterization to quantify the design trades between thruster performance and discharge channel wall robustness. Table 3 summarizes the major test phases.

Table 3: Summary of major thruster testing phases for the NASA-H64M-LM and the NASA-H64M-LMW.

Phase	Thruster	Description	Duration [hr]
A	LM	Performance and stability characterization: *200 to 600-W discharge power, 200 to 350-V discharge voltage, magnetic and cathode flow fraction mapping*	27
B	LM	Short duration wear: *500-W, 300-V discharge condition*	275
C	LM	Performance and stability characterization: *200 to 600-W discharge power, 200 to 350-V discharge voltage, magnetic and cathode flow fraction mapping*	5
D	LM	Thermal characterization: *300 to 600-W discharge power, 300 and 350-V discharge voltage*	18
E	LM	Accelerated wear characterization: *500-W, 300-V discharge condition*	108
F	LMW	Performance and stability characterization: *300 to 700-W discharge power, 300 and 350-V discharge voltage, magnetic and cathode flow fraction mapping, integrated demonstration with breadboard discharge module*	10
		Cumulative Thruster Operation	**443 hrs**

All major test phases except for Phase E are presented in this paper. Results from Phase E will be presented as part of a future publication.

A. Vacuum Test Facilities

Vacuum test facilities utilized during the NASA-H64M-LM's development included GRC's VF-8 and VF-56. The VF-8 facility, shown in Figure 17, is a 1.5-m diameter, 4.5-m long chamber whose pumping train (including four 35-inch diameter oil diffusion pumps) can achieve a base pressure of ~4 x 10^{-7} Torr. A displacement-style, inverted-pendulum thrust stand of heritage GRC design [14] was installed in VF-8 and tuned for low-thrust measurements with a maximum uncertainty [15] of ±2 %. Cathode testing for the NASA-H64M-LM was conducted in VF-56. This facility is a 0.9-m diameter, 0.9-m long chamber, whose cryopump can achieve a base pressure of ~5 x 10^{-6} Torr. Laboratory power supplies, diagnostics, and data acquisition systems were used throughout all experiments with some exceptions during integrated system testing.

Figure 17: GRC's VF-8 test facility utilized for NASA-H64M-LM thruster testing.

B. Thruster Performance Characterization

Performance and stability characterization of the NASA-H64M-LM thruster were performed in GRC's VF-8 vacuum test facility. Performance was measured at fourteen operating conditions, with discharge powers ranging from 200 to 600 W and discharge voltages ranging from 200 to 350 V. Most testing was performed with the thruster in an electrically floating configuration, but thruster-ground and cathode-tied electrical configurations were also evaluated for selected operating points. At each operating point, magnetic mapping was conducted across a dynamic range of 2.4X to assess discharge stability. The cathode flow fraction was also varied from 5 to 11% for selected operating points.

Figure 18 shows an example dataset of results for the thruster at beginning-of-life (BOL) with performance-optimized magnetic field strengths, a cathode flow fraction of 7%, and an electrically floating configuration. These test results were obtained at operational facility pressures of ~30 μTorr or lower. The total thruster power is the sum of the discharge and magnet powers, and the total specific impulse includes both the anode and cathode mass flow rates. Due to the use of a displacement-style thrust stand, the maximum uncertainty on the thrust measurements is ±2%. Uncertainty propagation yields a maximum uncertainty of ±3% and ±5% on specific impulse and thruster efficiency values, respectively. Overall performance values compare favorably against state-of-the-art Hall-effect thrusters in the same power class.

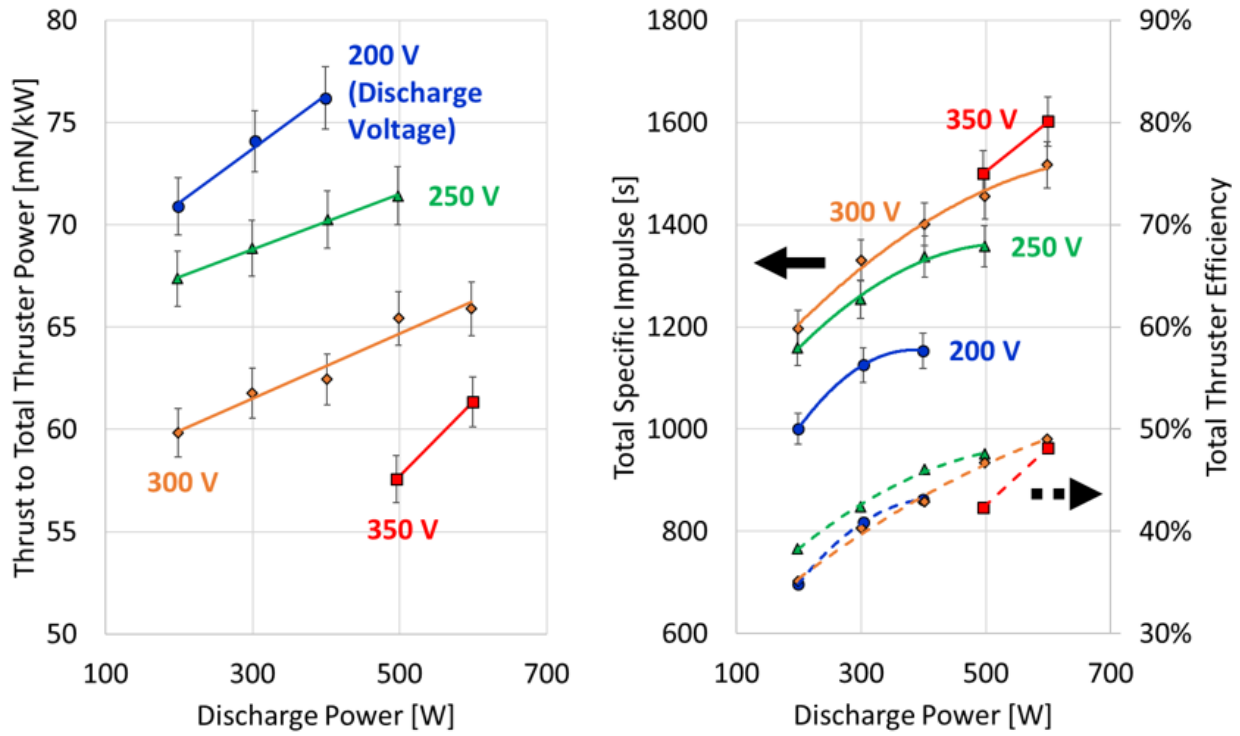

Figure 18: NASA-H64M-LM performance at beginning-of-life (BOL) with performance-optimized magnetic field strengths, 7% cathode flow fraction, and electrically floating configuration. The total thruster efficiency uncertainty bars (up to a maximum of ±5%) are not shown for clarity.

A wider-channel modification (15% wider) of the NASA-H64M-LM thruster also underwent performance and stability characterization to assess the tradeoffs between thruster channel width and discharge channel wall robustness. Having a wider discharge channel reduces inefficiencies due to wall losses and permits higher-power operation, while maintaining similar plasma current density. The major drawback is that the wider the channel, the thinner and more fragile the ceramic discharge channel walls are that would be subjected to significant shock and vibration during normal spaceflight launch and operational environments. The NASA-H64M-LMW thruster modification was made by machining away the inner channel wall material of a spare NASA-H64M-LM discharge channel. No modifications were made to the magnetic circuit or other thruster features.

Performance and stability characterization of the NASA-H64M-LMW were performed in GRC's VF-8 vacuum test facility at operating facility pressures of ~30 μTorr or lower. The thruster was operated at 300 and 350-V discharge voltages up to 700-W discharge power. Initial test results suggest that, particularly for higher-power operations, an optimal SSEP thruster design is likely to be one with a slightly wider channel than the baseline NASA-H64M-LM. Table 4 summarizes the improvement in performance observed between the NASA-H64M-LM and the NASA-H64M-LMW modification at 600-W discharge power.

Table 4: Summary of NASA-H64M-LMW performance improvement in comparison to NASA-H64M-LM at BOL 600-W discharge power, 7% cathode flow fraction, and performance-optimized magnetic field strength.

Discharge Voltage [V]	*Thrust to Total Thruster Power*	*Total Specific Impulse*	*Total Thruster Efficiency*
300	1.03X	1.06X	+4%
350	1.02X	1.04X	+3%

More details regarding the performance, stability, and wear characterization of both thruster configurations are anticipated for a future publication.

C. Thruster Wear Characterization

Following BOL characterization of the NASA-H64M-LM, the thruster was operated at the 500-W, 300-V discharge condition until a total thruster operational time of 300 hours was reached. Performance and stability characterization of the thruster were then repeated at fourteen operating conditions with the thruster in an electrically floating configuration. At each operating point, magnetic mapping was conducted across a dynamic range of 2.4X to assess discharge stability. Figure 19 shows an example set of results for the thruster at BOL + 300 hr, with the same magnetic field settings as the data in Figure 18 and a cathode flow fraction of 7%. These test results were obtained at operational facility pressures of ~30 μTorr or lower.

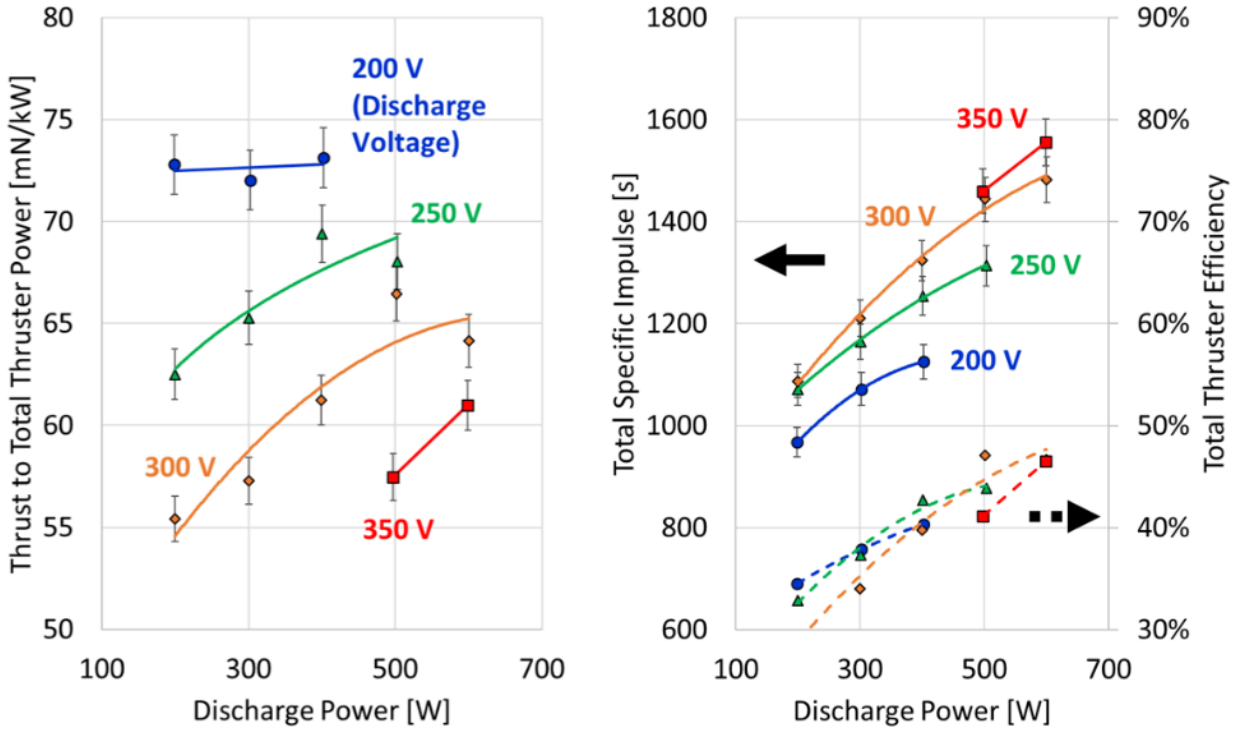

Figure 19: NASA-H64M-LM performance at BOL + 300 hr with the same magnetic field settings as the results in Figure 18, 7% cathode flow fraction, and electrically floating configuration. The total thruster efficiency uncertainty bars (up to a maximum of ±5%) are not shown for clarity.

After 300 hours of operations, the NASA-H64M-LM displayed slightly lower performance compared to BOL, as typically expected during Hall-effect thruster early operation. Although, at the higher-power operating points for the 300 and 350-V discharge voltages, where the NASA-H64M-LM is nominally optimized to operate, the performance degradation after extended thruster operation is modest. This trend can be readily seen in Figure 20, which considers the 300-V discharge data from Figure 18 and Figure 19.

Performance for the 300 and 350-V operating conditions presented in this paper is summarized in Table 5 for easy reference. The total specific impulse accounts for both the anode and cathode propellant flows. The total thruster efficiency η_T is defined as

$$\eta_T = \frac{g_0}{2}\frac{TI_{sp}}{P_T} \tag{3}$$

where T is the measured thrust, g_0 is the sea-level gravitational constant, and P_T is the total thruster power (i.e., sum of the discharge and magnet powers).

Wear of the thruster discharge channel was measured with a chromatic, white-light non-contact benchtop profilometer. The employed profilometer is equipped with an optical pen oriented normal to the thruster exit plane with a 3-mm measuring range. Measurement of the discharge channel erosion was made by centering the thruster on the erosion measurement fixture and then performing radial profile scans at the various azimuthal locations. The measured profiles were then compared to the discharge channel BOL configuration. Preliminary analysis of the thruster's discharge channel measured erosion rates indicate erosion rates that are consistent with the thruster's

projected propellant throughput capability of greater than 100 kg. Details on these measurement are anticipated to be presented in a future publication.

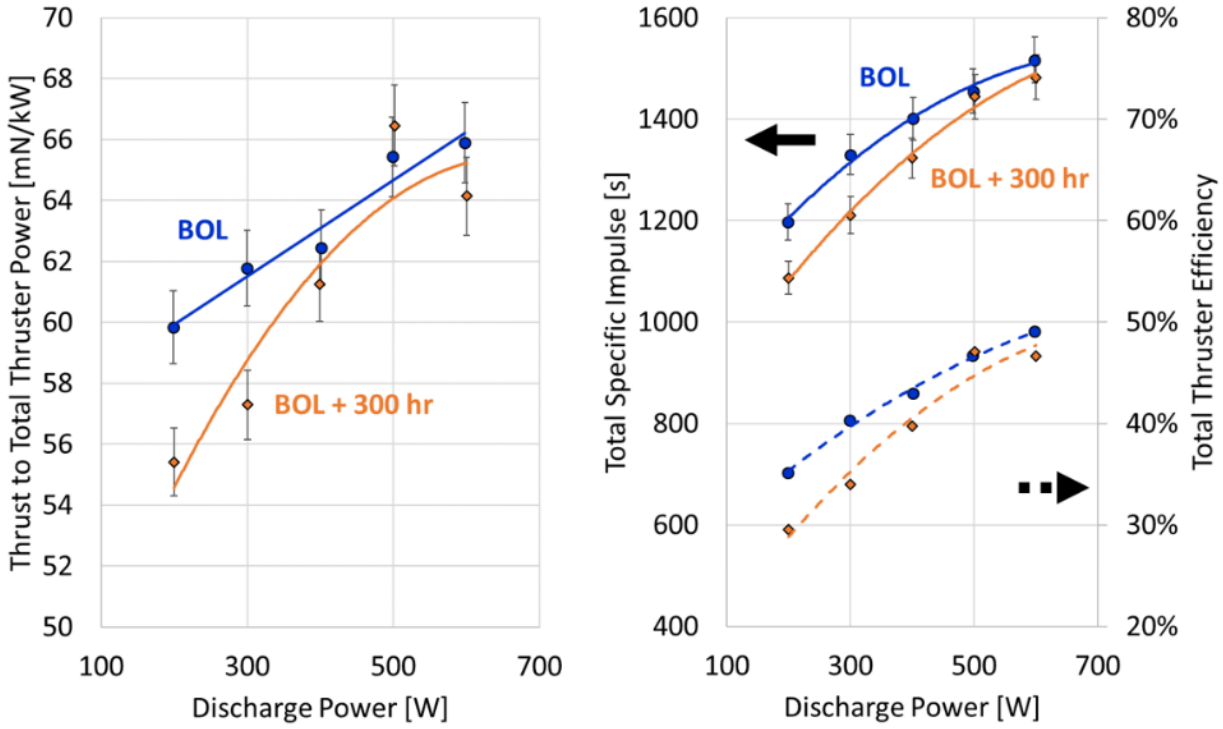

Figure 20: Comparison of NASA-H64M-LM performance at BOL versus BOL + 300 hr for 300-V discharge voltage, identical magnetic field settings, 7% cathode flow fraction, and electrically floating configuration. The total thruster efficiency uncertainty bars (up to a maximum of ±5%) are not shown for clarity.

Table 5: Summary of 300 and 350-V NASA-H64M-LM and NASA-H64M-LMW thruster performance at 7% cathode fraction as presented in this paper. Maximum uncertainties are ±2% for thrust, ±3% for specific impulse, and ±5% for efficiency.

Thruster Configuration / Condition	Discharge Power [W]	Discharge Voltage [V]	Thrust [mN]	I_{sp} [s]	η_T
LM BOL	500	300	33	1455	47%
LM BOL	600	300	41	1517	49%
LM BOL	500	350	29	1500	42%
LM BOL	600	350	38	1601	48%
LM BOL + 300 hr	500	300	34	1444	47%
LM BOL + 300 hr	600	300	40	1483	47%
LM BOL + 300 hr	500	350	29	1460	41%
LM BOL + 300 hr	600	350	37	1555	47%
LMW BOL	600	300	42	1602	53%
LMW BOL	700	300	48	1608	53%
LMW BOL	600	350	38	1671	51%
LMW BOL	700	350	44	1702	52%

D. Thruster Thermal Characterization

Typical Hall-effect thrusters see temperature swings from -40 °C to 600 °C during regular operation on plasma wetted components, with cathode temperatures exceeding 1000 °C. As such, careful thermal design is a key consideration during any thruster development. In addition, Hall-effect thrusters are commonly constructed from a

variety of metals and ceramics with differing coefficients of thermal expansion (CTE). Generally for electric propulsion systems, heat dissipation on orbit favors passive modes. As such, heat generated by the internal components must be conducted to the exterior surfaces of the thruster for rejection via radiation. Nearly all of these conductive paths can have multiple interfaces that must be designed to efficiently transfer heat, yet mitigate thermal stresses, particularly in the ceramic components.

Development of a detailed thermal model of the thruster assembly correlated to test data is a practical and efficient method to predict the temperatures of all components and thermal impacts of design decisions. For the NASA-H64M-LM, a computational thermal model was developed to ensure that the design has sufficient heat dissipation and that components remain within allowable temperature limits under all operating and environmental conditions. This model, accounting for the entire thruster assembly as well as all conductive and radiative exchange of thermal energy, was developed in a commercially available thermal modeling software by expanding on modeling techniques used on prior NASA GRC Hall-effect thrusters [16].

For the thermal model, resistive heating of the magnetic coil windings were applied based on observed thruster magnet power requirements at steady-state operating conditions. A sub-model of the cathode assembly was constructed to estimate heat loads from the emitter necessary for sustained cathode operation. Plasma heating on thruster surfaces was initially estimated based on prior Hall-effect thruster development data and then subsequently adjusted during model correlation to match H64M-LM thruster measured temperatures.

The resultant model yields steady-state solutions to estimate peak temperatures as well as transient solutions to predict temperature profiles during thruster start-up, operational changes, and cool-down. Figure 21 shows an example result of the NASA-H64M-LM's thermal simulation at the 500-W, 300-V discharge operating condition.

To conduct thermal model correlation, the NASA-H64M-LM was instrumented with 17 thermocouples and tested in GRC's VF-8 facility at 307 operational hours after beginning-of-life. These thermocouples were placed in critical locations to aid with refining modeled interface contact conductances among the thruster components. Thermal test data was acquired with the thruster operating from 300 to 600 W, and the modeled emittance values of the thruster exterior were revised to account for observed surface quality and facility backsputter. The resultant correlation yields good agreement between the model predictions and the thermocouple data. For example, at the 500-W, 300-V discharge operating condition, steady-state model predictions are within 5% of the test data and show large thermal margins on component temperature limits, including the inner coil windings at the highest thruster magnetic field setting. Via correlation with test data, this tuned thermal model becomes available to support further thruster development.

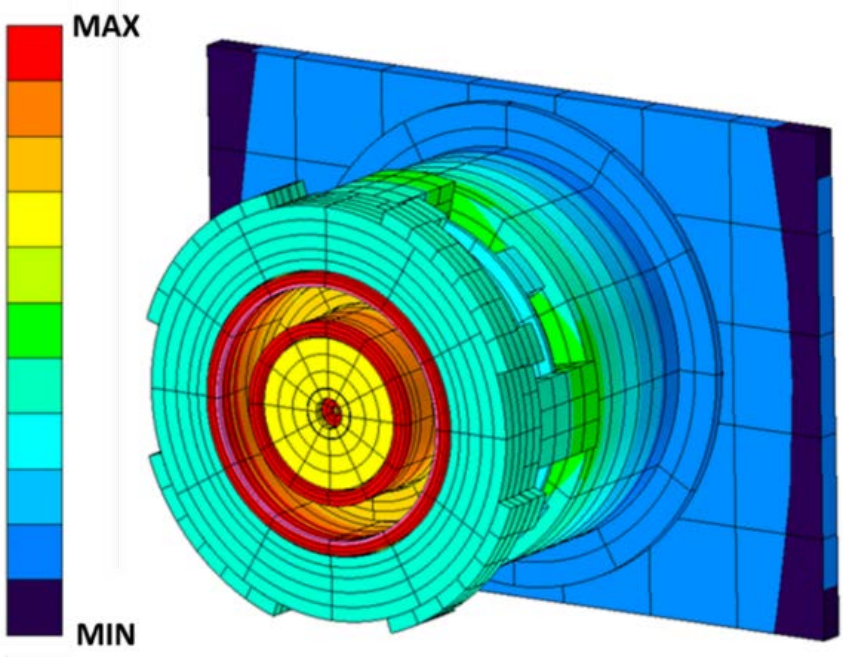

Figure 21: Steady-state thermal model results for NASA-H64M-LM operating at a 500-W, 300-V discharge in which all heat is dissipated to the environment via radiation.

VIII. HT-SSEP Integrated System Demonstration

An integrated system (i.e., thruster and single discharge breadboard module) demonstration was performed with the wider-channel variant (NASA-H64M-LMW) thruster. This demonstration was conducted in GRC's VF-8 vacuum test facility with the thruster body electrically floating. The thruster discharge was powered by the breadboard module, while the electromagnets, cathode keeper, and cathode heater were powered using laboratory supplies. Figure 22 shows a picture of the thruster during operation.

Figure 22: NASA-H64M-LMW operating in VF-8.

The thruster was lit using a glow-discharge startup procedure with the breadboard module, followed by ramping of the electromagnets until the breadboard achieved the 300-W, 300-V discharge condition. The nominal single module discharge supply design output is 375 W. Thruster performance at this operating condition is summarized in Table 6 and is in good agreement with prior test data acquired with a laboratory discharge power supply. The breadboard module's discharge voltage was then increased to 350 V to assess the voltage output capability of the single breadboard discharge module. No anomalies were observed during the voltage ramp, during which the discharge current rose by 1%, while xenon flow rates were kept constant. Because this particular operating point had not been previously explored, no comparison data using a laboratory power supply is provided.

Table 6: Comparison of NASA-H64M-LMW (wider-channel variant) thruster test data using laboratory and breadboard discharge supplies.

Discharge Supply	Discharge Power [W]	Discharge Voltage [V]	Cathode Flow Fraction	Thrust [mN]	Chamber Pressure [μTorr]
Laboratory Power Supply	299	300	7.4%	17.8 ± 0.4	13
Breadboard Module (Integrated Test)	292	299	7.3%	18.2 ± 0.4	13
Breadboard Module (Integrated Test)	347	351	7.3%	19.7 ± 0.4	12

To assess the current output capability of the single breadboard discharge module, the thruster's anode flow was systematically incremented, while the discharge voltage was fixed at 300 V. Thruster operations were successfully maintained up to a discharge current of 1.32 A (or 395-W discharge power), at which point the breadboard's over-current protection was tripped. Figure 23 shows the voltages and currents sourced by the breadboard discharge module during the integrated demonstration. High-speed voltage and current data acquired during the tests provided useful discharge module coupling data that is being incorporated into a refined design of the SSEP discharge module. Following the single breadboard demonstration, minor modifications were implemented and two additional modules were manufactured along with the master controller. The three-module configuration has been demonstrated using resistive loads, and an integrated demonstration with the H64M thruster is anticipated in the near future.

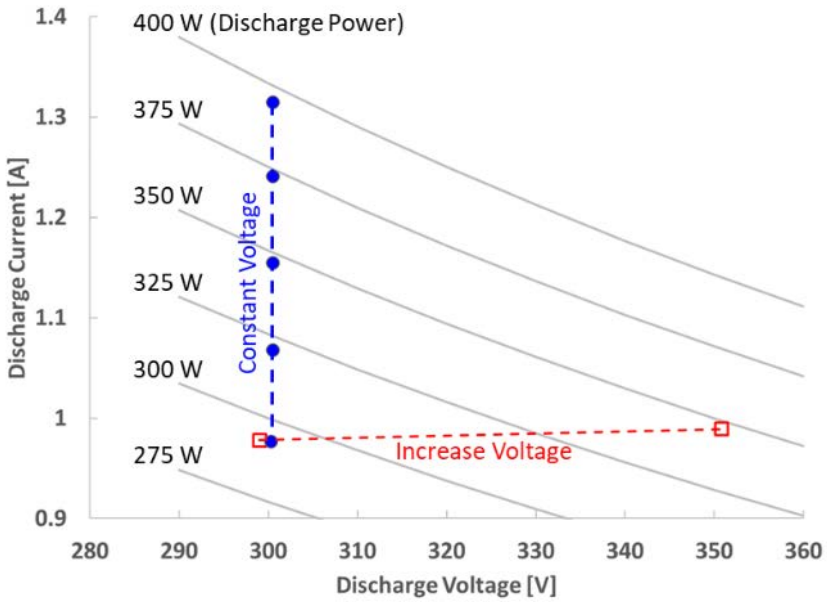

Figure 23: Performance space of a single SSEP breadboard discharge module explored during integrated demonstration with the NASA-H64M-LMW thruster.

IX. Conclusions

NASA Glenn Research Center engineering expertise, fabrication capabilities, and world-class test facilities in the field of electric propulsion facilitated the aforementioned work to be completed in one year in a single design iteration with incredible success. Thrusters of similar capability to the H64M have taken multiple iterations to achieve similar performance and TRL.

The high propellant throughput electric propulsion system advanced under the SKEP project has addressed key NASA and industry stakeholder needs, mitigated important technology development risks, and outlined a clear path-to-flight. The thruster and PPU work leveraged numerous prior NASA investments and produced many creative innovations to solve the unique challenges of developing a miniaturized, long-life Hall-effect electric propulsion system for small spacecraft.

Pending continued funding, GRC aims to finish delivering an initial high total impulse capability for NASA small spacecraft science missions through collaborations with industry. The ultimate goal is to make the described thruster and PPU designs available domestically to credible electric propulsion developers on a non-exclusive basis. Building on the test results from the H64M, opportunities identified for further cost and technical risk reduction, and added margin to meet collective stakeholder needs, the H71M-EMP (Engineering Model Pathfinder) design was initiated in late fiscal year 2018. GRC continues to seek opportunities to complete the HT-SSEP development, provide NASA with technology enabling lower-cost science missions, and transfer the resulting technology to domestic industry.

Acknowledgments

Numerous NASA GRC civil servants and contractors have painstakingly supported the HT-SSEP work described in this paper. The authors would like to thank Dean Petters and Tim Smith for project management; David Jacobson for technical leadership; Deb Waters for test facility management; Mike Depauw, Rich Senyitko, Nick Lalli, and Sandra Doehne for test facility leadership; Randy Clapper for design support; Matt Baird for PPU requirements development support, Jaime Scibelli for market research support, Tom Tomsik and Ryan Gilligan for feed system concept support; Bill Fabanich for thermal modeling support; Ariel Dimston for structural engineering support; Riniah Foor and the GRC fabrication shop for going above and beyond to fabricate hardware in a timely fashion; Kevin Blake and Josh Gibson for thruster assembly support; Mike Arnett, James Sadey, Tom Haag, Tom Ralys, Matt Daugherty, and Roland Gregg for test facility engineering and preparations; ZIN Technologies for engineering support, principally in PPU breadboard fabrication and testing, including Chris Sheehan, Andrew Browser, Brian Bellisario, and Charlie Druesedow; Pete Peterson, Randy Duvall, and Eric Overton for risk mitigation; and Holly Walburn for administrative support. The work accomplished in 12 months was nothing short of astonishing.

X. References

[1] NASA, "NASA 2018 Strategic Plan," NASA Headquarters, 2018.

[2] NASA, "Small Spacecraft Technology - State of the Art," NASA/TP–2018-220027.

[3] Goebel, D. M. and Katz, I., *Fundamentals of Electric Propulsion: Ion and Hall Thrusters*, Jet Propulsion Laboratory, 2008.

[4] McGuire, M. L., Hack, K. J., Manzella, D. H. and Herman, D. A., "Concept designs for NASA's Solar Electric Propulsion Technology Demonstration Mission," 50th AIAA/ASME/SAE/ASEE Joint Propulsion Conference, Cleveland, OH, AIAA-2014-3717.

[5] Baranov, V., Nazarenko, Y., and Petrosov, V., "Azimuthal Non-Uniformities in Accelerators with Closed Electron Drift," IEPC-2001-018.

[6] Reid, B. M., "The Influence of Neutral Flow Rate in the Operation of Hall Thrusters," Ph.D. dissertation, University of Michigan, 2009.

[7] Huang, W., and Yim, J., "Propellant Distributor for a Thruster". USA Patent 10,273,944, 30 April 2019.

[8] Patterson, M. J., Foster, J. E., Haag, T. W., Pinero, L., and Soulas, G. C., "Ion propulsion development activities at the NASA Glenn Research Center," 39th AIAA/ASME/SAE/ASEE Joint Propulsion Conference, AIAA-2003-4709.

[9] Domonkos, M. T., Gallimore, A. D., and Patterson, M. J., "Parametric Investigation of Orifice Aspect-Ratio on Low Current Hollow Cathode Power Consumption," 34th AIAA/ASME/SAE/ASEE Joint Propulsion Conference and Exhibit, Cleveland, OH, AIAA 1998-3345.

[10] Williamson, W. S., Dulgeroff, C. R., Williams, R. L., and Bayless, J. R., "8-cm Engineering Model Thruster Technology: A Review of Recent Developments," 14th International Electric Propulsion Conference, Princeton, New Jersey, AIAA-1979-2103.

[11] Patterson, M. J., Domonkos, M. T., Carpenter, C., and Kovaleski, S. D., "Recent Development Activities in Hollow Cathode," 27th International Electric Propulsion Conference, Pasadena, California, IEPC-2001-270.

[12] Kohl, W. H., *Handbook of Materials and Techniques for Vacuum Devices*, New York: Reinhold, 1967, p. 494.

[13] Ham, R. K., Williams, J. D., Hall, S. J., Benavides, G. F., and Verhey, T. R., "Characterization of propellant flow and bias required to initiate an arc discharge in a heaterless hollow cathode," 55th AIAA/SAE/ASEE Joint Propulsion Conference, Indianapolis, IN, 2019.

[14] Haag, T. W., "Thrust Stand for High-Power Electric Propulsion Devices," Review of Scientific Instruments, Vol. 62, No. 5, 1991.

[15] Mackey, J. A., Haag, T. W., Kamhawi, H., Hall, S. J., and Peterson, P. Y., "Uncertainty in Inverted Pendulum Thrust Measurements," NASA/TM-2018-219952.

[16] Myers, J. L., Kamhawi, H., Yim, J. T., and Clayman, L. K., "Hall Thruster Thermal Modeling and Test Data Correlation," 52nd AIAA/SAE/ASEE Joint Propulsion Conference, Salt Lake City, UT, AIAA-2016-4535.